Regular Article

Characterisation of polyphosphate coated aluminium-doped titania nanoparticles during milling

Laura N. Elliott [a,b,*], Juliette S. Behra [a], Nicole Hondow [a], Richard A. Bourne [a,c], Ali Hassanpour [a], John L. Edwards [d], Stephen Sutcliffe [d], Timothy N. Hunter [a]

[a] School of Chemical and Process Engineering, University of Leeds, Leeds LS2 9JT, United Kingdom
[b] Centre for Doctoral Training in Complex Particulate Products and Processes, University of Leeds, United Kingdom
[c] Institute of Process Research and Development, School of Chemistry, University of Leeds, United Kingdom
[d] Venator, Titanium House, Hanzard Drive, Wynyard Park, Stockton-on-Tees TS22 5FD, United Kingdom

HIGHLIGHTS

- Particle fines (10–20 nm) were observed after milling TiO₂ for 32 min, with no change in crystal phase.
- DLS data confirmed the hydrodynamic diameter is relatively unchanged with milling time.
- NMR relaxation rate enhancement is observed for longer milling times, due to phosphate content changes.
- Elemental analysis shows a difference in polyphosphate content for washed and unwashed samples.

GRAPHICAL ABSTRACT
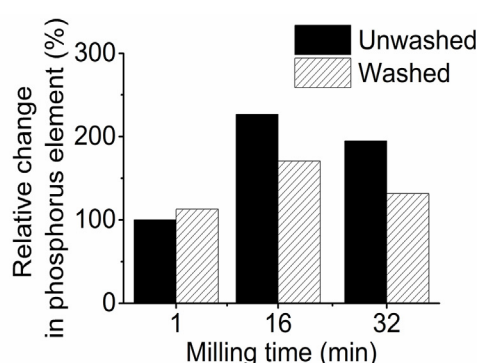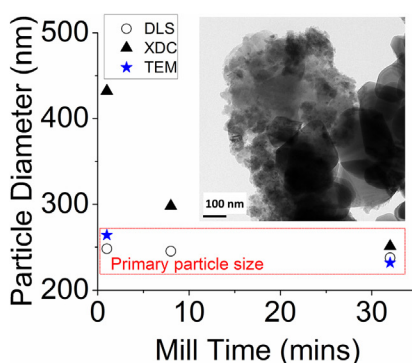
ARTICLE INFO

ABSTRACT

This paper investigates the characterisation of alumina-doped titania nanoparticles, milled under high-shear over time, in the presence of sodium hexametaphosphate (SHMP) dispersant. Transmission electron microscopy (TEM) indicated that prolonged milling times led to the formation of 10 nm particle fines which were electrostatically attracted to larger particles, where no change in the crystal structure was observed. Primary particle sizes measured by dynamic light scattering (DLS) and TEM were in agreement and showed no change in primary particle size ($\sim$250 nm) with respect to milling time, however, there was a clear reduction in the magnitude of the slow mode decay associated to aggregates. The TiO₂ was found to have an isoelectric point (iep) in the range of pH 3–4.5, where an increase in milling time led to a lower pH_{iep}, indicative of an increase in SHMP coverage, which was further supported by an intensification in phosphorus content measured by X-ray fluorescence (XRF). Phosphorus content and zeta potential analysis before and after centrifugal washing showed that SHMP was partially removed or hydrolysed for the longer milled pigment samples, whereas no change was observed for shorter milled samples. Relaxation NMR was also performed, where enhanced relaxation rates at longer milling times were associated partially to increases in surface area and exposure of Al sites, as well as physicochemical changes to SHMP density and structure. It is thought that extended milling times may lead to hydrolysis or other structural changes of the dispersant from the high energy milling conditions, allowing easier removal after washing for longer milled pigments.

* Corresponding author.
    E-mail address: pmlne@leeds.ac.uk (L.N. Elliott).

1. Introduction

Titanium dioxide (TiO$_2$), commonly called titania, occurs in three abundant crystallographic forms, rutile, anatase and broo-kite [1,2], and is a key pigment used in a wide range of consumer products such as paints, cosmetics, pharmaceuticals and plastics [3–6]. The estimated market in 2014 was 6 million tonnes, worth approximately US$ 13.5 billion globally [7]. TiO$_2$ can be produced by two main routes, the *chloride* and *sulphate* processes. Commercial pigment type rutile titania is primarily produced by the chloride process, which was commercialised by DuPont in the 1950's [6,8].

Dopants are regularly added during the chloride process. For example, small quantities of AlCl$_3$ are added to the reactor feed to control pigment aggregation and favour the rutile phase [2,8,9]. It has been proposed that some Al dissolves into the titania lattice which enhances the phase transformation rate [10,11]. Later in the production process, titania is subjected to various chemical surface treatments to improve durability and dispersibility, before being wet milled to control the particle size distribution and dried. The final quality of TiO$_2$ in consumer products is dependent on a number of these variables where, in particular, the size of the milled dispersed crystallite aggregates is a key physical parameter that dictates overall whiteness and brightness [6,8,12].

Polyphosphate salts are widely used as dispersants in mineral and material processing industries, due to their ability to adsorb onto metal-oxides and clay-particle surfaces including illite, mont-morillonite, kaolinite and dolomite [13–16]. Hence, polyphosphates are also often added to the titania pigment suspension during processes such as milling, in order to improve the dispersion properties and reduce suspension viscosity [17]. Taylor *et al.* [17] investigated polyphosphate interactions with alumina doped rutile pigment particles, and showed under alkaline conditions (pH 9) the interactions are dominated by chemisorption, whilst at pH 4 a combination of chemisorption and electrostatic interaction occurs. Feiler *et al.* [18] and Michelmore *et al.* [19] both studied the adsorption of polyphosphates onto the surface of TiO$_2$ and SiO$_2$ particles. For TiO$_2$, it has been shown that increasing the concentration of polyphosphate [18] and/or increasing the chain length of the linear polyphosphate [19] led to a decrease in the magnitude of the zeta potential at pH 4, but no interactions were observed for SiO$_2$. Connor [20] studied phosphate adsorption onto titanium dioxide films by *in situ* infrared spectroscopy and adsorption kinetics, and suggested that phosphate strongly binds as a bidentate surface species. Importantly, aqueous polyphosphate solutions are not stable under high temperature (above 120 °C), acidic pH, or in the presence of some metal ions [21], as covered in recent reviews by Cini [22] and Rashchi [23]. Farrokhpay *et al.* [24–26] have investigated the stability and the influence of polymeric and polyphosphate dispersants on titania pigment particles. They found that acidic conditions (pH 3.5 – 5.5), high calcium ion concentrations and elevated temperatures all decreased the polyphosphate dispersion properties of titanium pigment particles [26].

Although efforts have been made to understand the influence of dispersants on slurry rheology during milling (see review by He *et al.* [27]), there appears to be limited published research studying polyphosphates. Wang and Forssberg [16] studied the interactions of sodium hexametaphosphate (SHMP) with dolomite in a stirred bead mill. They found that the use of SHMP, compared to organic dispersants, led to particles of a larger mean size and lower surface area. However, to our knowledge, the influence of milling time on the structure and density of polyphosphate dispersants on the surface of titania pigment particles has not yet been explored, nor has there been any published research relating to the strength of the interactions through centrifugal washing.

A number of studies have been conducted on the milling of TiO$_2$ particles (without polyphosphates) to determine the optimum milling control parameters, such as agitation speed, mill ball size, filling ratio and suspension concentration [28–31]. Interestingly, Inkyo *et al.* [31] found that large beads (50 and 100 μm) did not effectively break up nanoparticle agglomerates, although the structure and morphology of the nanoparticles were altered with milling time, moving from rod-shaped to more spherical morphologies. Jeon *et al.* [32] compared the wet milling of titania with alumina, and they reported that increased milling times led to alumina aggregates becoming more worm-like, whereas titania particles remained fairly spherical.

Phase transformations have also been reported for high energy ball milling of anatase with prolonged milling times. Begin-Colin *et al.* [33] showed, using TEM, that polycrystalline particles formed with TiO$_2$-II grains at the surface of the anatase particles after 15 min of milling. Gajovic *et al.* [34] also reported a phase transformation from anatase to TiO$_2$-II, as investigated by Raman spectroscopy and TEM. Sen *et al.* [35] observed particle fines 40–50 nm in size after ball milling anatase for 32 h, and after milling for 100 h they observed disintegration of nanoparticles to sizes of ∼13 nm. Both anatase and rutile have also been observed to transform into TiO$_2$-II with shear [36]. For example, Šepelák *et al.* [36] observed TiO$_2$-II crystallites of 10 nm in diameter on the surface of anatase particles using high resolution TEM. However, to date, formation of nanoparticle fines from milling of rutile phase titania has not been reported.

TiO$_2$ particle size is important, as this controls the amount of scattered light. The optimum mean size is around 200 nm because the sum of the light scattered at each wavelength reaches its maximum [6,8,12]. Currently, TiO$_2$ pigments are manufactured in a continuous process with concentrations up to 600 g/L, and the particle size is often monitored using dynamic light scattering (DLS) [37]. Concentrated slurries exhibit multiple scattering; which leads to significant errors in the measured sizes and cannot be accounted for by most of the commonly available DLS devices [38]. Thus, to monitor the size of TiO$_2$ particles by DLS during a production process, aliquots must be sampled and diluted to concentrations where no multiple scattering occurs. Not only is this time consuming, but samples may be misrepresentative of the bulk system if an insignificant amount of statistics is collected on the dilute system or if particle aggregation/agglomeration occurs.

Studying industrially relevant processes is often not straightforward, as the dispersions are commonly highly concentrated, opaque and may contain a variety of inorganic contaminants [9]. However, nuclear magnetic resonance (NRM) relaxometry can be used to determine particle specific surface area, even for highly concentrated slurries [39]. In contrast to DLS, surface area calculations from relaxometry data do not require any assumptions on particle size or shape [39,40]. Furthermore, the NMR technique allows particles to be measured in the wetted state, contrary to most surface area techniques such as Brauner-Emmett-Teller (BET), that are performed on dried samples which are often subjected to aggregation. Relaxation NMR is thus an ideal candidate for an online process control tool, and could, for instance, offer the possibility of continuously monitoring particle surface area during milling.

Solvent relaxation NMR has been used to study the adsorption of polymers and dispersants onto particles and shows changes in the relaxation rate of bound water at the particle interface [39,41–50]. The technique has been used to determine particle porosity [51–54]. However, its use for surface area measurements is limited [39,55–57]. Elliott *et al.* [58] demonstrated that relaxation NMR can be used to measure the surface area of TiO$_2$ samples of different crystal structures (with the use of a standard silica

reference material of a known surface area) and showed excellent agreement with BET. Cosgrove *et al.* [49] studied relative relaxation rates for alumina (surface charge density 0.42 μCcm^{-2}) and latex (1.6 μCcm^{-2}). They showed that the time bound water spends at the surface of a particle is not entirely determined by the surface charge of the particle. In the case of alumina particles, despite a lower surface charge compared to latex, a larger increase in relaxation rate is observed. Thus, indicating a faster relaxation of bound water at the alumina particle surface due to surface hydroxyl groups which causes the motional restriction of water through specific interactions. This type of unproportionable increase in relaxation rate is often called a relative relaxation rate enhancement. Thoma *et al.* [55] investigated two titania powders consisting of aluminosilicate coated rutile of pigment grade quality. They reported deviations for highly concentrated slurries due to a decrease in the signal to noise ratio from the NMR, because of a reduction in the number of protons present in the system.

This paper presents the characterisation of industrially produced alumina-doped TiO_2 pigment particles milled for different periods of time in the presence of a polyphosphate salt. It aims to understand how milling affects the aggregate size and morphology of alumina-doped rutile pigment particles through particle size characterisation by TEM, X-ray disc centrifugation (XDC) and DLS. Further we investiagte how the surface density and structure of the polyphosphate salt change with milling time. The stability of the polyphosphate layer against centrifugal washing is investigated by studying changes in the zeta potential and phosphorus content using XRF. Additionally, we explore the use of NMR relaxometry as a novel technique to understand changes in surface area in real time during the milling process and understand the influence of the polyphosphate-alumina interactions on relaxation times.

2. Materials and methods

2.1. Materials

Unmilled and milled titanium dioxide pigment samples were supplied by Venator. Sodium hexametaphosphate (Univar), known by the trade name Calgon, and abbreviated as SHMP throughout this manuscript, was added prior to the milling process to control titania dispersion properties. Stock acid and base solutions were prepared to vary the pH of suspensions, where hydrochloric acid (Sigma-Aldrich, reagent grade, 37%) was used to decrease the pH and potassium hydroxide pellets (Sigma-Aldrich) were used to increase the pH. Pure potassium chloride salt (Sigma-Aldrich) was used as background electrolyte for surface charge analysis. A copper sulphate solution (Xigo Nanotools) was used as received to calibrate the frequency prior to NMR resonant frequency measurements. Ethanol absolute was purchased from Fisher Scientific and used as received for TEM sample preparation.

2.2. Methods

The industrially produced pigment samples were firstly adjusted to pH 10–10.5 with NaOH and sodium hexametaphosphate (SHMP) was added prior to milling at 0.14% w/w as P_2O_5 on TiO_2. Suspensions were milled at concentrations of 400 g/L in a stirred wet lab-scale mill (60 mL total volume) using a rotor speed of 12,000 RPM. The conditions in the mill were designed to mimic industrial-scale media mills commonly used in comminution of tiania for pigment. The milling media used was grade 8 ballotini with a mean size of 500 μm. Aliquots of TiO_2 were

removed after 1, 2, 4, 8, 16 and 32 min of milling and dried in an oven at 105 °C.

The so-obtained dried titania powder was heavily agglomerated due to capillary forces, and in order to handle the samples for dispersion characterisation, they were gently crushed using a mortar and pestle for 5 min. All suspensions were made in milli-Q water and dispersed using an ultrasonic bath (Clifton Sonic) for 30 min, unless otherwise stated. Samples were then further dispersed using an ultrasonic probe, a Sonic Dismembrator (Fisher Scientific), at 20% amplitude for 1 min using a 6 mm horn tip.

Some of the milled samples were washed post-milling in an attempt to remove poorly adsorbed SHMP, and these are stated as *washed* herein. For these samples, 2.5 wt% dispersions were prepared in ultrapure water and centrifuged using a Heraeus Megafuge 16R Centrifuge (Thermo Scientific). Two wash cycles were performed. The first one was carried out at 6000 RPM for 20 min, after which the supernatant was removed and conductivity measured using a Seven2Go S3 (Mettler Toledo). The concentration of the centrifuged samples were adjusted back to 2.5 wt% using ultrapure water and washed for the second time at 8,000 RPM for 20 min. Once again the supernatant was removed, conductivity was measured, and the washed particles were re-dispersed to 2.2 wt%.

2.2.1. Transmission electron microscopy (TEM)

Samples of TiO_2 milled for 1 and 32 min were prepared for TEM by suspending in ethanol and vigorously shaking, before a drop of the dispersion was placed onto a copper grid coated with a holey carbon film (Agar Scientific Ltd.) and left to dry. TEM analysis was used to investigate primary particle size and crystal structure on FEI Tecnai F20 FEGTEM operating at 200 kV. Bright field TEM was used to investigate particle size and morphology with images collected on a Gatan Orius CCD. Particle size analysis was conducted using Image J [59] by measuring the Feret diameter of primary particles. High magnification TEM images were used to obtain distances between atomic planes using a fast Fourier transform (FFT) function, from which d-spacings were then measured.

The dispersion state of TiO_2 nanoparticles after 32 min of milling was further investigated by dispersing in water, and using the plunge-freeze and vacuum dry method, as previously described by Hondow *et al.* [60]. Briefly, this involved rapidly freezing a blotted 3.5 μL droplet onto continuous carbon coated TEM grids which had been plasma cleaned (1020 Fischione) for 10 s. The droplet was blotted using an FEI Vitrobot, with prior conditions set to 100% relative humidity and 21 °C in the chamber. After a wait time of 10 s, the droplet was blotted once for 4 s. The blotted droplet was rapidly plunged into liquid ethane, stored in liquid nitrogen, then transferred into a vacuum desiccator and allowed to sublime.

Energy dispersive X-ray spectroscopy (EDS) was used as elemental analysis for TiO_2 before after milling for 32 min (plunge-frozen and vacuum dried) to check for potential bead contamination from milling media, and to confirm the presence of the polyphosphate species on the alumina-doped pigment surface. EDS was performed using the SuperX (4 detector) system on the FEI Titan[3] G2 operated at 300 kV. High angle annular dark field (HAADF) scanning TEM (STEM) images were recorded using a probe current of ~450 pA, with analysis performed using the Bruker Esprit (v1.9) software.

2.2.2. X-ray diffraction (XRD)

Titanium dioxide samples were analysed after 1 and 32 min milling. The X-ray powder diffraction patterns were obtained to investigate the nature of the crystalline phase and calculate the crystallite sizes, using a D8 X-ray Diffractometer (Bruker) and CuKα radiation source. The titanium dioxide samples were prepared as powders and deposited onto a silicon holder. The samples

were scanned from 2θ angle 10° to 70° with a step size 0.0490° at 304 ms per step. The obtained pattern was matched against anatase [61] and rutile [62] crystal structures, which were also used to index the d-spacing measured from TEM analysis.

Crystallite size, L (Å), was obtained using the Scherrer equation [63] (Eq. (1)), where B is the line broadening in the XRD peak at the full width half maximum intensity (FWHM) after subtracting instrumental line broadening (radians). Here, the line broadening of the instrument was taken as 0.06°, and the FWHM was obtained by fitting a Gaussian distribution to the two most intense peaks observed in the XRD patterns. K is a dimensionless shape factor; a value of 0.89 was used as this relates to spherical particles [63]. $\chi/2$ is the Bragg angle (radians) which was obtained from the peak position at the FWHM, and λ the wavelength of the incident x-rays taken as 1.5406 Å for the CuKα radiation source.

$$B = \frac{K\lambda}{L\cos\frac{\chi}{2}} \tag{1}$$

2.2.3. Zeta potential characterisation

A Zetasizer Nano ZS (Malvern Instruments) was used to measure the zeta potential of the unmilled and milled dispersions. Dispersions of TiO$_2$ in 0.1 mM KCl background electrolyte were prepared at 100 ppm and dispersed as per Section 2.2, where the pH was measured using a HI-208 pH meter (Hanna Instruments), before pipetting into DTS1070 folded capillary cells (Malvern Instruments). Stock base (KOH) and acid (HCl) solutions were prepared at 0.01, 0.1 and 1 M, to increase and decrease the pH of the particle dispersions respectively. The pH of the dispersion was either reduced from neutral with acid or increased with base. All dispersions were kept mixing with a magnetic stirrer for approximately 10 min after altering the pH. The zetasizer standard operating procedure (SOP) was set for 3 measurements with a maximum of 100 profiles, and measurements automatically terminated when 10 stable profiles were sequentially collated. A total of 6 measurements were collected for each pH point on the zeta potential curve, and averaged data were recorded with associated standard deviation and error.

2.2.4. Dynamic light scattering (DLS)

Titanium dioxide suspensions were prepared from the milled powder at 2 wt% in ultrapure deionised water and dispersed, as per Section 2.2. 25 μL aliquots were sampled and diluted in 20 mL of ultrapure deionised water and re-dispersed, before diluting by ten. The dispersions were filtered using 0.80 μm surfactant-free cellulose acetate filters (26 mm Minisart® Syringe filters; Sartorius), unless otherwise stated. This sample preparation was also used for TiO$_2$ milled for 1, 16 and 32 min after centrifugal washing. The DLS measurements were performed at 25 °C also using a Zetasizer Nano ZS (Malvern Instruments, 173° backscattering angle and 633 nm laser excitation wavelength). For each suspension, thirty 30 s measurements were carried out.

For all the investigated milled suspensions, the collected intensity auto-correlation data exhibited two relaxation modes. As seen in Fig. S1(a) of the Supplementary Material, the fit of the data performed by the commercial Zetasizer code did not properly account for the second, longer, relaxation mode. The intensity auto-correlation data were thus fitted in MatLab with a sum of two stretched exponentials (Eq. (S1)) using the Levenberg-Marquardt algorithm. An example of such a fit is provided in Fig. S1(b). It is worth noting that the few measurements for which the intensity auto-correlation data had an intercept higher than 1 were excluded from the data set, while the remaining intensity auto-correlation data were normalised to an intercept of 1. Assuming that the investigated relaxation mode is diffusive (see a more detailed explana-

tion in Section 3.2 and in the Supplementary Material), corresponding hydrodynamic diameters D_H were calculated using Eqs. (S1)–(S5). More information on DLS fitting and analysis procedures can be found in Behra *et al.* [64].

Care must be exercised when characterising TiO$_2$ suspensions with light scattering as they can exhibit multiple scattering because of the TiO$_2$ high scattering index (*i.e.* 2.410). Multiple scattering leads to significant errors in size measurements if it is not accounted for and can be avoided by diluting TiO$_2$ suspensions. To determine the optimum TiO$_2$ concentration at which DLS measurements should be performed [37,38], dilution trials were attempted. The results are shown and discussed in the Supplementary Material (Fig. S3), where the influence of filtration is also discussed. The concentration corresponding to the dilution described at the beginning of this section (*i.e.* ~2.5 × 10^{-3} wt%) was found to be optimal. To confirm that this concentration was appropriate, a number of additional measurements were performed using a light scattering device equipped with a '3D mode' (instrument details provided in the Supplementary Material), which allows to correct for multiple scattering [37,64]. There was no significant difference between the data collected with the '3D mode' (data not shown) and those collected with the standard '2D mode', thus confirming that the selected TiO$_2$ concentration allowed DLS measurements to be performed in absence of multiple scattering.

There was a concern that the amount of energy brought into the system during sonication could break the aggregates that may be present in the TiO$_2$ milled samples. Hence, DLS measurements were also performed on samples prepared using a lower energy intensive dispersion method (compared to sonication). The results are displayed in Fig. S4 and show that sonication does not break the aggregates that may be present in solution, but successfully breaks the agglomerates formed when the TiO$_2$ milled particles are dried. These experiments are discussed in detail in the Supplementary Material. Characterisation of the unmilled TiO$_2$ sample is also detailed in the Supplementary Material, Section 1.6, Fig. S5.

2.2.5. X-ray disc centrifugation (XDC)

Milled slurries obtained at ~400 gL^{-1} were diluted to ~40 gL^{-1} and the titanium dioxide particle size was determined by X-ray disc centrifugation using a BI-XDC Particle Size Analyzer (Brookhaven), run at a disc speed of 1200 rpm for 40 min.

2.2.6. Brunauer–Emmett–Teller (BET)

Brunauer–Emmett–Teller (BET) surface area and pore size measurements were obtained for milled titanium dioxide samples by the nitrogen adsorption-desorption method at 77.3 K, using a TriStar 3000 (Micromeritics) surface analyser. TiO$_2$ samples were degassed to remove moisture using a vacuum oven at 120 °C for 24 h under a vacuum of 10 mmHg. To determine the reproducibility of the results, two TiO$_2$ samples (1 and 2 min milled) measurements were repeated using the same experimental conditions. No significant difference was observed for the 1 min milled sample (a 0.02% variation) or the 2 min milled sample (a 0.16% variation), with repeated results within the experimental error. The obtained N$_2$ adsorption isotherms were used to calculate the BET parameters for TiO$_2$ surface area, whilst the desorption isotherms were used to calculate the average pore size by the Barrett-Joyner-Halenda (BJH) method.

2.2.7. NMR relaxometry

All relaxation measurements were obtained using an Acorn Area (Xigo Nanotools), 13 MHz desktop NMR spectrometer. Prior to any operation, the instrument was thermally equilibrated for 24 h, after which the resonance frequency was measured using a copper sulphate solution. A resonance frequency of approximately 13.07 MHz is regarded as adequate for a measurement to proceed.

A 90°-pulse length of 5.67 μs, 180°-pulse length of 11.33 μs and a gain value of 10 dB were used for all relaxation measurements. The T_1 inversion recovery pulse sequence was used to measure the spin–lattice relaxation rate coefficient, and a Carr–Purcell–Mei boom–Gill (CPMG) pulse sequence was used to measure the spin-spin T_2 relaxation. Typically, a series of four replicate scans were averaged to produce the CPMG trace, and the Xigo Nanotools software fitted the collected signal to a single exponential to extract the relaxation rate coefficient. A recycle delay of 5 T_1 between scans was used. An anticipated value for T_1 was estimated for each milled sample and the software calculated a geometric series of 11 values of τ in order to span the relevant experimental interval to determine T_1. An iterative process was initially used to determine an anticipated T_1 to within 20% of the "true value". Three T_2 or T_1 values were measured and averaged per TiO$_2$ sample.

Suspensions were prepared at 2.5 wt% in deionised water as previously described. The specific surface area (S) of milled titanium dioxide samples were calculated using the theory discussed by Elliott *et al.* [58] and Fairhurst *et al.* [39] (see Eqs. (2) and (3)). The average relaxation time (T_{av}) of the TiO$_2$ dispersions were used to calculate the average relaxation rate (R_{av}) of the dispersion. The solvent (deionised water) relaxation time was measured (T_b) and converted into a solvent relaxation rate (R_b). A relaxation rate enhancement (R_{sp}) was calculated for the milled TiO$_2$ dispersions, (see Eq. (2)), using both R_{av} and R_b.

$$R_{sp} = \frac{R_{av}}{R_b} - 1 \qquad (2)$$

$$S = \frac{R_{sp}R_b}{K_a\psi_p} \qquad (3)$$

The R_{sp} was plotted against the particle volume ratio (Ψ_p) and the gradient of the line of best fit obtained. The specific relaxation constant (K_a) for milled TiO$_2$ was calculated by equating the surface area to that obtained from the BET measurement for the 8 min milled sample, giving a K_a of 3.93×10^{-4} g/m^2/ms. Washed TiO$_2$ samples were also characterised with this procedure, but at a concentration of 2.2 wt% (due to sample loss during the washing procedure). In order to compare R_{sp} values to those of the 2.5 wt% unwashed samples, the T_1 relaxation rate was measured and converted into R_{sp}, and the equivalent R_{sp} value for a corresponding 2.5 wt% slurry was back calculated from the R_{sp}/ψ_p gradient.

2.2.8. X-ray fluorescence (XRF)

Washed and unwashed TiO$_2$ dispersions at 2 wt% were prepared as described in the introduction of Section 2.2. The dispersions were poured into plastic holders ensuring that there was enough volume to cover the surface of the cup. Cup holders (40 mm Spex Unicell) were covered with a polypropylene film to contain the sample before securing with the plastic ring counterpart, creating a taut smooth film on the surface of the sample cup. XRF measurements were performed in a helium atmosphere using a Rigaku Primus II WD XRF. The following settings were used; analysis: EZ scan, sample type: liquid, component type: metal and balance component: H$_2$O.

3. Results and discussion

3.1. Microscopy, elemental characterisation and crystal structure

Transmission electron microscopy (TEM) images (Figs. 1 and 2) were obtained for TiO$_2$ particles in order to understand primary particle size and morphology changes within the two extreme milling times (after 1 min and 32 min respectively). It is noted that a large proportion of primary particles are rod shaped, while there is certainly some considerable variation in their shape factors. Jordan *et al.* [65] analysed the self-assembly of rutile TiO$_2$ during initial stages of crystallization, where they reported elaborate structures of rutile TiO$_2$, such as rutile fibre networks and twinning branched clusters [65,67], although it should be emphasised that an alternative synthetic route is used for the samples in this study. Klein *et al.* [66] stated that synthesis acidity is important in determining crystal morphology of rutile titania when produced by the precipitation method, and detailed structures including rods, broomlike agglomerates and cauliflower spherical agglomerates. Clearly, the morphology of the nanoparticles depends on the conditions used, however observed in this study are spheres and rod shaped nanoparticles limited to TiO$_2$ produced in a flame reactor. It is assumed that the variation in shape-factors evidenced in Figs. 1 and 2 are likely from a distribution in growth rates, rather than differences in the underlying crystalline structure, which will be discussed in detail in the forthcoming section.

It should be noted that throughout this discussion the term 'aggregate' is referred to as an assembly of particles which are sufficiently strongly bound that they require bead milling to break the particle-particle bonds. This contrasts to the term 'agglomerate'
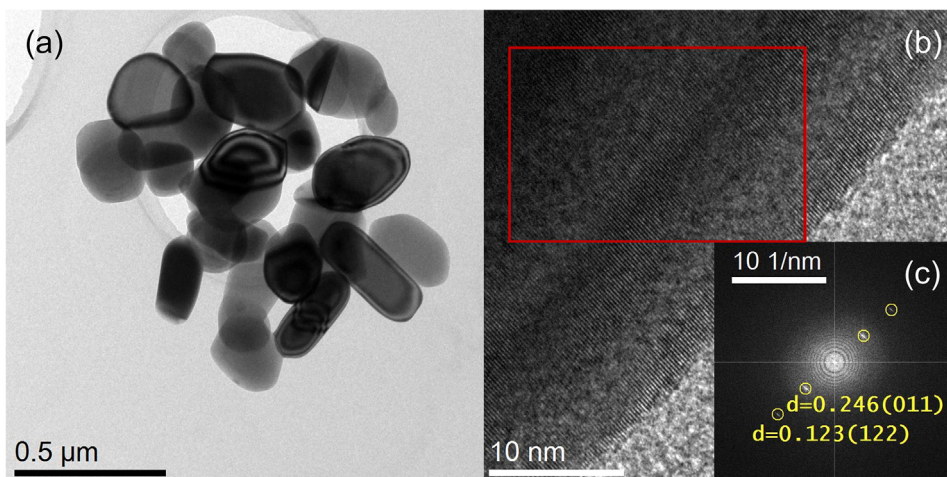
Fig. 1. (a) TEM image of TiO$_2$ particles after milling for 1 min. (b) High magnification image of a TiO$_2$ nanoparticle after 1 min of milling to show the lattice fringes. (c) Fast Fourier transform (FFT) generated from the red square shown in (b), with measured d-spacings in nm and corresponding hkl planes shown referenced to the rutile crystal structure [62].
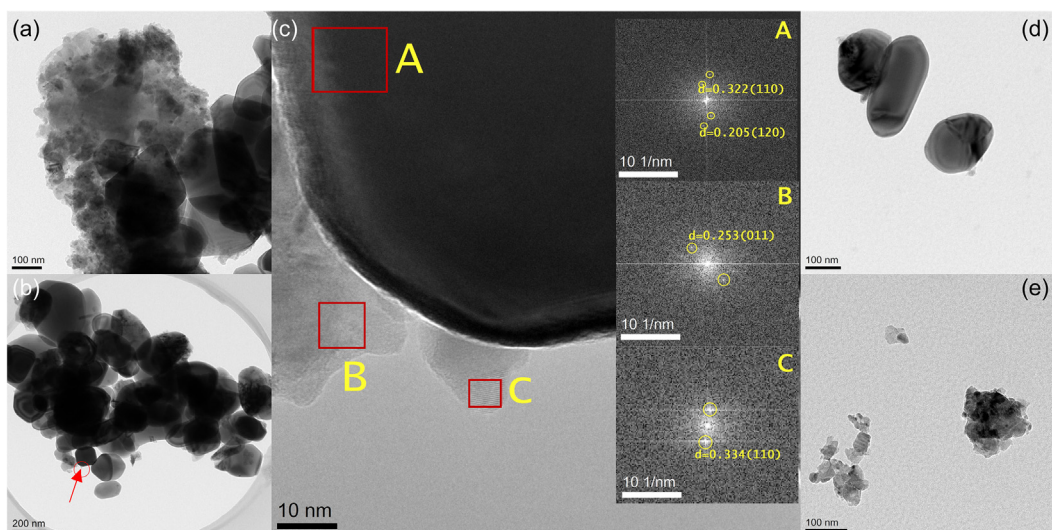
Fig. 2. (a & b) TEM images of TiO₂ particles after milling for 32 min (particle fines electrostatically aggregated highlighted by the arrow in (b)). (c) High magnification TEM image at the point of the arrow in (b), with inset FFT taken from A, B and C sections indicated by the red box insets, with measured d-spacings and corresponding hkl planes shown [62]. (d & e) TEM images indicating the dispersion state of TiO₂ after milling for 32 min, dispersed in water and prepared using the plunge-freeze method.

which is referred to as a collection of aggregated particles which has formed upon drying, these are softer bound and as later discussed can be broken by sonicating the suspension.

The average particle size was calculated using the Feret diameter of the TiO₂ primary particles, with over 100 particles measured for the unmilled material and both the 1 and 32 min milled samples, as given in the Supplementary Material, Table S1. Little change is observed in the average primary particle size between the unmilled pigment and size with increased milling time. A small number of aggregates (10) were analysed which had an average spherical diameter equivalent of ~1100 nm after 1 min milling and 900 nm after 32 min milling. While it is expected that there may be some level of particle aggregation in TiO₂ slurries [67], the observed aggregates could also have formed during sample drying on the TEM grid. Hence, the measured aggregate sizes are unlikely to be representative of the aggregates that may be present in the wet dispersions.

Critically, titania samples milled for 32 min showed evidence of particle fracturing (Fig. 2), resulting in fines of ~20 nm, which appear to cluster together (Fig. 2a) and are also attached to larger particles (Fig. 2c), probably due to electrostatic attraction [35]. Sen *et al.* [35] found particle fines in the order of 40–50 nm in size after high energy vibrational ball milling of anatase nanoparticles for 32 h, where further milling for 100 h caused disintegration of nanoparticles to sizes of ~13 nm [35]. They suggested that particle breakage is caused by critical stresses that generate plastic deformation. It has also been observed that high energy ball milling results in the formation of uncommon metastable TiO₂-II phase. Gajovic *et al.* [68] also showed that milling times of more than 10 h for the anatase polymorph induced particle breakage towards 10 nm, while primary particles of larger sizes were still present [68]. Therefore, it appears that for the current system, 32 min milling supplies an excess milling energy, which not only is inefficient on time/energy costs, but negatively impacts the properties of the pigment particles. It is likely that the observed nanoparticle fines will lead to a reduction in the optical purity and whiteness. This is the first time, to the authors' knowledge, that such breakage has been published for the harder rutile morphology (hardness scale anatase 5.5 – 6, compared to rutile 6–6.5) [69]. Although the milling conditions are fairly sever, such large milling RPM are required in order to scale down the milling process from production plant-scale to lab-scale. Therefore, the appearance of fractured

TiO₂ fines is significant, as many pigment production processes will have similar unit operations, and thus it could be assumed that many TiO₂ samples may contain these fractured fines, when the TiO₂ reactor discharge is milled for long times.

The crystal structure of primary particles was investigated by analysis of lattice fringes in high magnification TEM images (Fig. 1b), and a fast Fourier transform (FFT) was generated to measure the d-spacing (Fig. 1c). The TiO₂ sample milled for 1 min had primary particles of the rutile crystal phase, as observed by the d-spacing corresponding to the (0 1 1) and the (1 2 2) planes of rutile [62], as shown in Fig. 1c. Due to crystal phase transformations reported in the literature after milling anatase TiO₂ [35], the crystal phase of the particle fines were also investigated for the 32 min milled sample. Fig. 2c shows three locations where the FFT was generated, either on the primary particle surface or on the fractured fines attached to the primary particle. The FFT generated from the primary particle (inset Fig. 2c, point A) again indicates d-spacings corresponding to the rutile (1 1 0) and (1 2 0) planes [62], and the fractured fines (inset Fig. 2c, points B and C) also have planes corresponding to the rutile (1 1 0) and (0 1 1) planes [62]. The dispersion behaviour of fractured fines was investigated for the 32 min milled TiO₂ sample, using the plunge-freeze and vacuum dry method described by Hondow *et al.* [60], allowing a closer *in situ* assessment of aggregation unaffected by sample drying. The fractured fines appear to either attach to the primary particle surfaces (Fig. 2d) or cluster together (Fig. 2e), thus suggesting that the fractured fines are not well dispersed in the suspension, which may significantly impact on the overall optical properties of the bulk material.

It was suspected that the ball milling media (glass ballotini) may contaminate the titania samples for extended milling times up to 32 min. Additionally, due to the industrial nature of the samples, other contaminants may also be present. Energy dispersive X-ray spectroscopy (EDS) was used as elemental analysis for the plunge-frozen 32 min milled sample, as presented in Fig. 3. It confirms the presence of silicon from the ballotini which is heterogeneously distributed across the particle. As the TiO₂ were milled in a slurry of sodium hexametaphosphate (SHMP), phosphorus and sodium are also evident, and appear to be evenly distributed on the surface. Dopants are regularly added during the chloride process. For example, small quantities of AlCl₃ (between 0.01 and 10%, although 0.5–2% is more typical), are added to the reactor feed
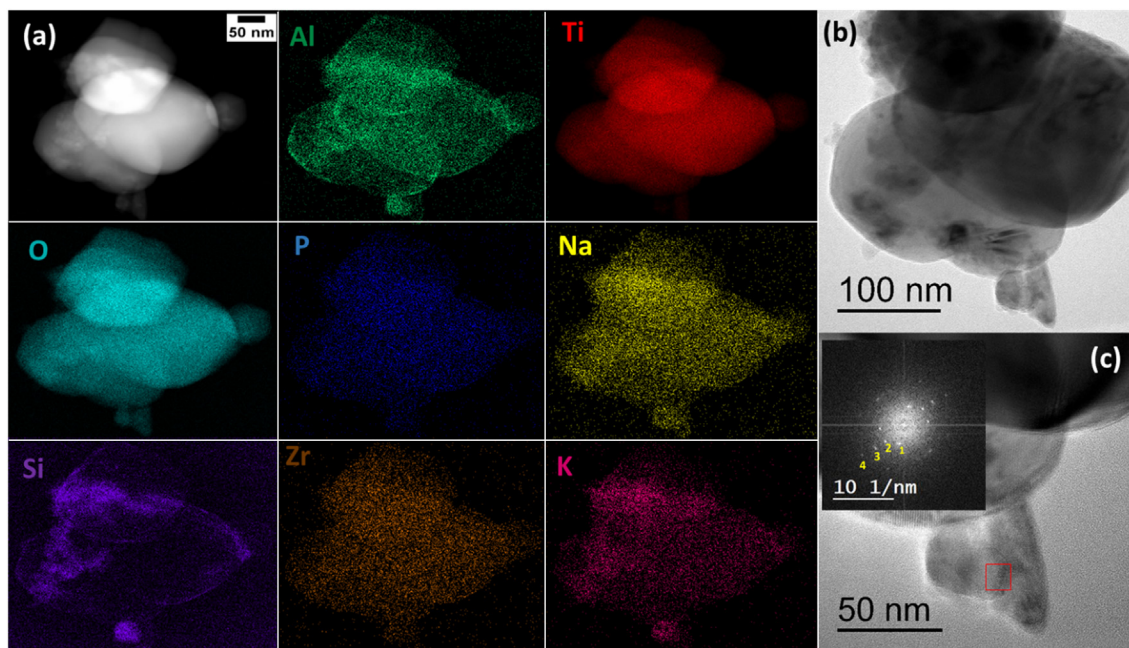
Fig. 3. (a) STEM image of TiO₂ milled for 32 min with EDS maps showing spatial distribution of relative elements. (b) TEM image of the TiO₂ sample prepared using the plunge-freeze vacuum dry method and (c) higher magnification TEM image showing fractured fines with inset FFT from the square highlighted. d-spacings corresponding to hkl rutile crystalline phase [62] measured from inset FFT; $d_1 = 0.340$ nm (1 1 0), $d_2 = 0.248$ nm (0 1 1), $d_3 = 0.170$ nm (1 2 1), and $d_4 = 0.121$ nm (1 2 2).

to control pigment aggregation and favour the rutile phase [2,8,9] and hence aluminium is also clearly evidenced on the particle surface. Finally, zirconia is also observed in Fig. 3, which is a result of contamination from degradation of the impeller used in the mill. Fig. 3(b) shows a TEM of the particles from which the EDS was mapped. Here, observed fines are again attached to the larger primary particle surface. Fig. 3(c) shows the FFT generated from an area on the fines that also confirms the rutile crystal phase with the d-spacing and hkl planes [62]. Additional EDS maps of the unmilled TiO₂ and 32 min milled particles are displayed in the Supplementary Material Figs. S6 and S7, which also shows an even coverage of the elements associated with the presence of SHMP on the TiO₂ particles.

Fig. 4 presents the XRD pattern of the TiO₂ samples after milling for 1 min and 32 min. Peaks again matched the rutile powder diffraction pattern [62], where no additional peaks were observed in the XRD pattern for both TiO₂ samples, further confirming phase and sample purity, although line broadening and a small shift in the peaks are detected. The peak broadening in the XRD was used to determine crystallite size for the two samples. Therefore, the two most intense peaks in the XRD pattern, (1 1 0) and (1 2 1), were fitted to a Gaussian distribution, as shown in Fig. 4 (b and c). Table 1 shows the full width half maximum (FWHM) obtained from the Gaussian fit and the calculated crystallite size using the Scherrer equation (Eq. (1)) [63]. The primary crystallite size marginally decreases with milling time from ~39–48 nm after milling for 1 min to ~35 nm after milling for 32 min, and this decrease suggests that stresses within the crystal structure leads to a broadening of the peaks.

The (1 1 0) peak at 2Theta ≈ 27° for rutile relates to the crystallite size of the shortest dimension, and the (0 0 1) or (0 0 2) plane corresponds to the longest dimension [70]. Length to width ratios of 2:1 are common for rutile crystals [70], which would give rise to crystallite lengths of ~100 nm. Although this is in closer agreement
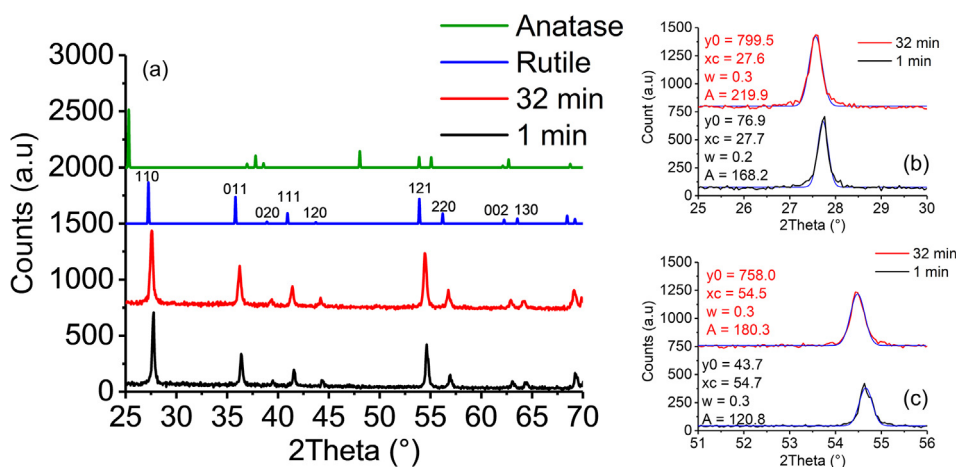
Fig. 4. (a) X-ray diffraction (XRD) pattern of 1 (black) and 32 min (red) milled TiO₂ samples compared to anatase [61] and rutile [62] crystal structures. (b) Expansion of (1 1 0) peak and (c) expansion of the (1 2 1) peak, both fitted to a Gaussian distribution with parameters y0 (baseline count), Xc (central 2Theta), w (peak width) and A (count amplitude). (For interpretation of the references to colour in this figure legend, the reader is referred to the web version of this article.)

Table 1
Crystallite sizes calculated from Gaussian fitting of the (1 1 0) and (1 2 1) XRD peaks for 1 and 32 min milled TiO$_2$.

| XRD peak	110	110	121	121
Milling time (min)	1	32	1	32
Position (°)	27.7	27.6	54.7	54.5
FWHM (°)	0.2	0.3	0.3	0.3
Crystallite size (nm)	48	36	39	35

with the primary particle sizes obtained from TEM, there is still a large discrepancy in the average crystal size. However, there are critical differences between direct primary particle size determination from TEM and crystal size characterisation by XRD, where primary particle sizes can only be measured by XRD if lattice planes are perfectly orientated [70]. Hence, under-estimation of particle sizes by XRD can occur, while it is clear that individual particles observed in the TEM do represent primary particles. In conclusion, no change in the primary particle size was observed with increased milling time, however there may be changes in the aggregate size. Longer milling times were found to induce particle fracturing resulting in nanoparticle fines 10–20 nm in size, although despite this, no change in the crystal structure was observed.

3.2. Particle surface charge and size changes through milling and washing

Zeta potential values for 1 and 32 min milled alumina doped TiO$_2$ in the presence of SHMP are presented in Fig. 5(a). Fig. 5(b) shows the evolution of the pigment zeta potential with milling time at neutral pH, before and after centrifugal washing. The investigated TiO$_2$ was found to have an isoelectric point (iep) between pH 3–4.5. With an increase in milling time leading to a lower pH$_{iep}$. Taylor et al. [71] previously reported a change in rutile iep with alumina doping, with pure rutile pH$_{iep}$ at 4.9. This contrasts to alumina doped rutile which they reported had a pH$_{iep}$ in the range of 8–9, dependent on the surface concentration of alumina. The change in iep is due to the domination of aluminium hydroxide surface groups [71]. However, while these values appear higher than those seen in Fig. 5, Taylor et al. [17], in other work, also reported the pH$_{iep}$ of pigmentary titania to vary significantly with the addition of SHMP, which even at low concentrations had a strong effect on the surface chemistry [17]. Indeed, they showed that the zeta potential decreased with polyphosphate concentration, which was pronounced at low pH (pH 4) and altered the reported pH$_{iep}$ to between 3 and 5, dependent on the dispersant concentration, consistent with values reported in Fig. 5 [17]. Further, Michelmore et al. [19] have shown that increasing the concentration of phosphate and increasing the chain length of the linear polyphosphate decrease the magnitude of the zeta potential of titanium dioxide.

Fig. 5(a) therefore suggests that increasing milling time leads to the presence of more SHMP on the alumina-doped pigment surface. It is expected that milling will lead to an increase in agglomerate breakage, potentially leaving more alumina-rich surface sites exposed. Thus, any non or poorly adsorbed dispersant remaining in the aqueous phase may adsorb to these newly exposed sites, leading to a reduced (more negative) zeta potential at low pH, because of the high charge density of the SHMP. Above pH 8 however, the zeta potential values remain constant near −50 mV regardless of milling time, consistent with Taylor et al. [17], and is indicative of the maximum potential magnitude of an adsorbed surface with SHMP.

Fig. 6 shows the XRF phosphorus elemental analysis for both washed and unwashed TiO$_2$ samples milled for different times. It
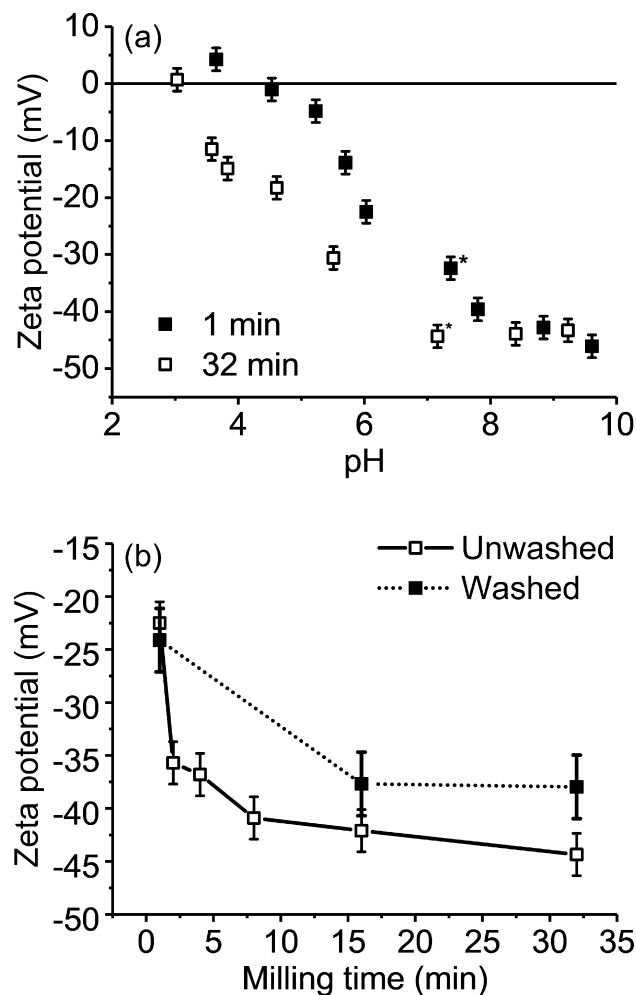
Fig. 5. (a) Zeta potential of aluminium doped TiO$_2$ particles in the presence of sodium hexametaphosphate (SHMP) for 1 and 32 min of milling. The neutral pH is indicated by (*). (b) Change in the TiO$_2$ zeta potential with milling time at neutral pH before and after centrifugal washing. In both (a) and (b), error bars represent the maximum standard deviation.

is important to note that the data has been first normalised to 100% Ti content, then the relative change in phosphorus calculated by setting the 1 min milled sample to 100% phosphorus content. The full elemental analysis obtained from XRF (which is also normalised to 100% Ti content) is given in the Supplementary Material (Fig. S8). There is a clear difference in phosphorus content for unwashed TiO$_2$ milled for 1 min, compared to 16 and 32 min of milling where the phosphorus content is relatively unchanged. Whilst it is clear that more phosphorus is in the samples milled for longer time periods, the exact quantity of phosphorus on the surface of TiO$_2$ is unknown due to the semi-quantitative nature of the technique. However, this change in phosphorus content supports the previous hypothesis that more SHMP is present on the pigment surface when milling time is increased. It is important to note that we cannot be certain from the XRF results alone that phosphorus is on the surface of the pigment. However, as previously discussed in terms of the EDS analysis as shown in Fig. 3, it is evident that phosphorus is spread over the particle surface rather than in the bulk solvent.

Additionally, there are important differences between washed and unwashed samples. From the XRF data (Fig. 6), washing does not induce a change in phosphorus content for the 1 min milled sample, while it leads to a significant decrease in the phosphorus content for the 16 and 32 min milled samples, inferring a partial
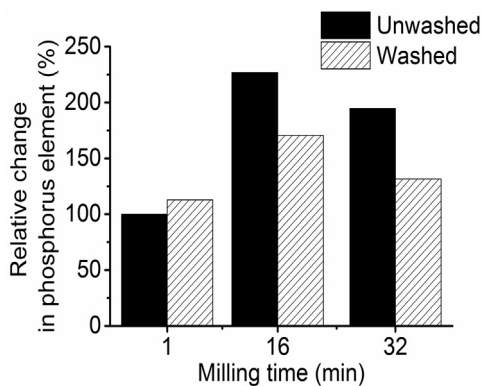
Fig. 6. X-Ray fluorescence data showing the relative difference in phosphorus content for 1, 16 and 32 min milled TiO$_2$ particles, before and after centrifugal washing. All XRF elemental data was first normalised by setting Ti mass% to 100%. The relative change in phosphorus content with milling time was calculated by setting the 1 min milled sample to 100% phosphorus content.

Fig. 7. Intensity auto-correlation data from DLS measurements of TiO$_2$ suspensions prepared from 1 (a) and 32 (b) minute milled samples. Thirty 30 s measurements were performed for each sample, and each is represented by a different colour symbol.

loss of the SHMP dispersant for samples milled at longer times. These results are consistent with zeta potential changes presented in Fig. 5(b), where, again, washing does not induce any change in the zeta potential for the 1 min milled sample, while it leads to a reduction in the magnitude of zeta potential for the 16 and 32 min milled suspensions. Hence, it appears that whilst milling increases the surface density of the dispersant, the SHMP that is additionally adsorbed is more easily removed upon washing.

The interaction of SHMP and titania can be complex, with both chemisorption (considered irreversible) and electrostatic physisorption (considered reversible) are possible [17]. It may be that the high energy of the mill induces some re-structuring and increases physisorption of the dispersant which is more weakly bound. Farrokhpay *et al.* [26] found that acidic pH, high calcium ion concentrations and elevated temperatures all decreased the ability of polyphosphate (Calgon T) to disperse titanium pigment particles of average primary particle size 230 nm. They concluded that the reduced dispersant performance, at least under high acid conditions and temperature, was due to the hydrolysis of the polyphosphate chains, which was observed through infra-red analysis. Furthermore, they reported that the reduction of the polyphosphate chain length from hydrolysis leads to a decrease in steric stabilisation, but the shorter chains still allowed electrostatic stabilisation to occur. Thus, we propose that mechanical activation at the pigment surface and high temperatures occurring during the milling process could either weaken the interaction between the adsorbed polyphosphate and the pigment surface, and/or cause the hydrolysis of the linear phosphate chains into shorter ones, thus allowing removal through centrifugal washing for the 16 and 32 min milled samples.

Fig. 7 presents the intensity auto-correlation data from DLS measurements of the 1 and 32 min milled TiO$_2$ suspensions, with 30 measurements collected for each sample (auto-correlation data for the unmilled sample is shown in Fig. S5). For all samples, two relaxation modes are observed: (i) a relaxation mode characterised by a short relaxation time of ~7 × 10^{-4} s at 173° scattering angle, independent from the milling duration, and (ii) a relaxation mode characterised by a significantly longer relaxation time varying from one measurement to another. Owing to their relaxation times, the first and second relaxation modes are termed 'fast' and 'slow' relaxation modes, respectively. The fact that two relaxation modes are probed by DLS suggests that two populations of particles are present in the suspensions. The presence of two particle populations was already suggested by the TEM images (see Section 3.1), where primary particles and aggregates of primary particles were
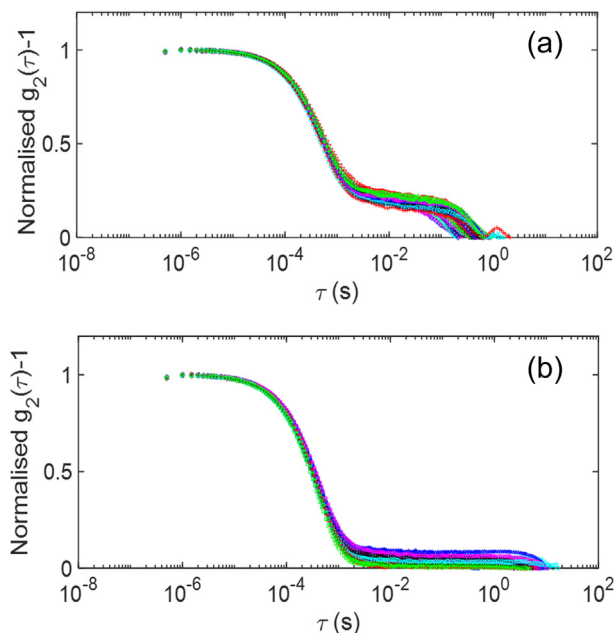
observed, though it could not be determined whether the aggregates were present in the TiO$_2$ suspensions or had formed during TEM sample preparation. It is worth noting that the DLS results do not rule out the formation of agglomerates during TEM sample preparation.

As discussed within Section 2.2.4 and in the Supplementary Material, the intensity auto-correlation data can be described by the sum of two stretched exponentials (one for each relaxation mode; see Eq. (S1) in the Supplementary Material); thus allowing the determination of the relaxation times associated to each relaxation mode. The fact that the slow mode relaxation times vary from one measurement to another suggests that the slow relaxation mode is associated with large polydisperse 'objects', and may be assigned to aggregates. Due to the inter-measurement variability of the slow relaxation time, no further calculation was performed for the slow relaxation mode.

The diffusive nature of the fast relaxation mode was confirmed with a light scattering device allowing DLS measurements to be performed at different scattering angles (see Supplementary Material and [64]). Hence, the hydrodynamic diameter D_H associated with the fast relaxation mode could be calculated from the fast relaxation time using the Stokes-Einstein equation (see Eqs. (S4) and (S5) in the Supplementary Material) and are shown in Fig. 8. Fig. 8 also compares the particle diameters obtained from X-ray disc centrifugation, TEM and DLS measurements. The hydrodynamic diameters determined from DLS measurements compare very well to the primary particle sizes measured from TEM (with measured diameters of ~250 nm almost unchanged with milling time) thus suggesting that the fast relaxation mode probed by DLS can be assigned to the primary TiO$_2$ particles. Fig. 8 also shows the ratio between the relative amplitudes of the fast and the slow modes (A_{fast} and A_{slow}, respectively) obtained by fitting the intensity auto-correlation data (see Eq. (S1) in the Supplementary Material). A_{slow}/A_{fast} decreases with milling time (and is greatest for the unmilled sample) thus suggesting a decrease in the proportion of aggregates with milling time compared to the primary particles.

Particle size determination from XDC, based on terminal settling described by the Stokes law, can be used to probe a wider
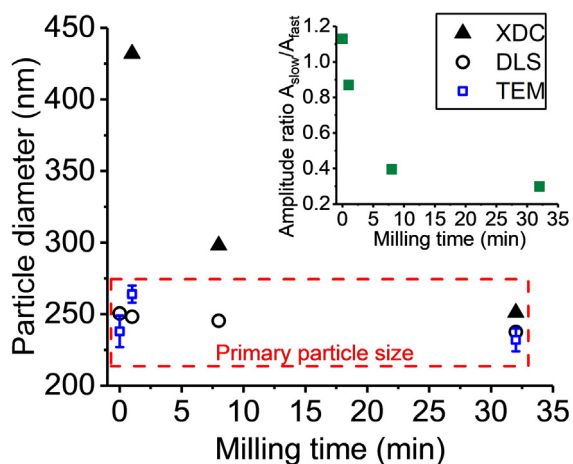
Fig. 8. Particle diameter of unmilled and milled TiO$_2$ particles measured using dynamic light scattering (DLS). Also shown is the particle size measured by x-ray disc centrifugation (XDC) and transmission electron microscopy (TEM). Additionally given is the ratio A_s/A_f of fast and slow mode relative amplitudes (from DLS measurements) as a function of milling time (inset). It should be noted that the amplitude of the slow mode for the unmilled sample was calculated by $(A_2 + A_3)/A_1$ where A_1 is the fast mode and A_2 and A_3 were the two additional slow modes present due to an increase in polydispersity.

Fig. 9. Brunauer–Emmett–Teller (BET) surface area for milled TiO$_2$ particles (left-hand side) with polynomial fit to guide the eye, and the calculated particle size based on a spherical shape (right-hand side) as a function of milling time.

range of sizes (*i.e.* ∼0.01–50 μm) than light scattering [72]. XDC results shown in Fig. 8 suggest an exponential-type decrease in particle or aggregate size with milling time. After 1 min milling, the measured size is ∼450 nm, which is assumed to be an average of the sizes of both primary particles and aggregates (considering that the primary particle size is ∼250 nm, as determined from TEM images). As the milling time is increased, the number of aggregates in the dispersion decreases, and the average particle size determined by XDC decreases towards that expected of the primary particles (∼250 nm). It is noted that, given the influences of particle shape [73,74] and aggregation [75] on sedimentation rate, XDC results must be taken with caution.

The hydrodynamic diameters of the washed and unwashed milled TiO$_2$ samples were determined using DLS and can be found in the Supplementary Material (Table S2), alongside the values of the A_{slow}/A_{fast} ratios. The hydrodynamic diameter associated with the fast relaxation mode does not change upon washing; consistent with the fact that the size of the primary particles is not expected to be affected by washing. For the 32 min milled TiO$_2$ sample, the value of A_{slow}/A_{fast} is not affected by washing, suggesting also that the proportion of aggregates are not considerably affected by washing. Such an observation would be consistent with partial hydrolysis of the polyphosphate during milling, maintaining the electrostatic stability of the system after partial removal of poorly bonded physisorbed dispersant with washing. Thus, the maintained layer is sufficient to continue to prevent primary particles from significant aggregation. Taylor *et al.* [17] state the SHMP molecular weight to range between 1082 and 1286 Daltons which would be a sufficient length to induce steric stabilisation.

3.3. Surface area determination and NMR relaxometry of milled samples

Fig. 9 presents the BET surface area plotted against the milling time. The specific surface area increases due to milling, from ∼5.7 m^2/g after 1 min milling to 7.5 m^2/g after 32 min milling, corresponding to calculated spherical equivalent diameters of 248 nm to 188 nm, respectively (as shown on the right-hand axis). The equivalent sizes calculated from BET surface areas are in relatively good agreement with the sizes estimated from TEM and DLS. Measuring shear-dependent aggregates is complex and it is important
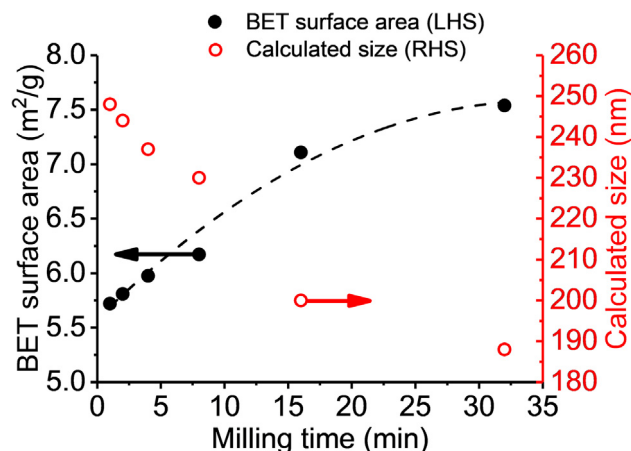
to use a variety of techniques to characterise the system. Gesenhues [76] also monitored surface area of rutile TiO$_2$ using BET, observing an increase in surface area from 6 to 8 m^2/g after 65 min milling. Other reported pigment TiO$_2$ surface areas are in the range of 8–9 m^2/g [17], 12–19 m^2/g [77,78] and can be as high as 28 m^2/g [79]. Mestl *et al.* [80] milled molybdenum oxide and showed crystallite size to be fairly constant in the first hour of milling, with a small decrease in particle size and an increase in BET surface area, suggesting the breakage of agglomerates and larger particles [80]. In the second phase of milling (milling times up to 600 min) the particle size drastically decreased, primary crystallites were broken down and amorphization occurred on their surface [80], all associated to an increase in the BET surface area. Thus, the results reported in Fig. 9 suggest that the increase in the specific surface area comes from aggregate breakage. The mean pore size obtained from BET measurements and the total pore volume (Supplementary Material, Table S3) remain constant ranging from 16 nm to 19 nm, further suggesting that the change in surface area is largely accounted for by the decrease in aggregate sizes. Some of the increase in surface area may also be accounted for by the formation of the nanoparticulate fines, although, as they are adsorbed on the dried agglomerated samples, it is likely that their influence on surface area changes is masked.

Changes in specific surface area, as measured by BET (in the dry state) were also compared to wet dispersion results from the NMR relaxometry measurements. Differences are observed in the NMR relaxation rate enhancement (R_{sp}; in reference to water) for the alumina-doped pigment particles as the milling time is increased, as shown in Fig. 10(a) (for unwashed dispersions). It is well known that the liquid bound at a particle surface has a relaxation time orders of magnitude shorter than the comparative bulk (2–3 s) due to molecular motion becoming anisotropic and restricted at the surface, thus increasing the relaxation rate [39,42]. Therefore, the increase in R_{sp} with respect to milling time also suggests an increase in surface area, which can be calculated from R_{sp} using a standard reference material of known surface area (see Section 2.2.7).

For dispersant-free suspensions of particles with identical surface chemistry, the relaxation rate scales linearly with increasing surface area [42]. However, adsorption of a dispersant at the particle surface may also lead to an increase in the relaxation rate, from the decrease in the mobility of water at the particle surface [42]. Due to the complexities of correlating the interactions of the dispersant to a separate calibration system of known surface area, the BET surface area for the 8 min milled samples was used to find K_a (the
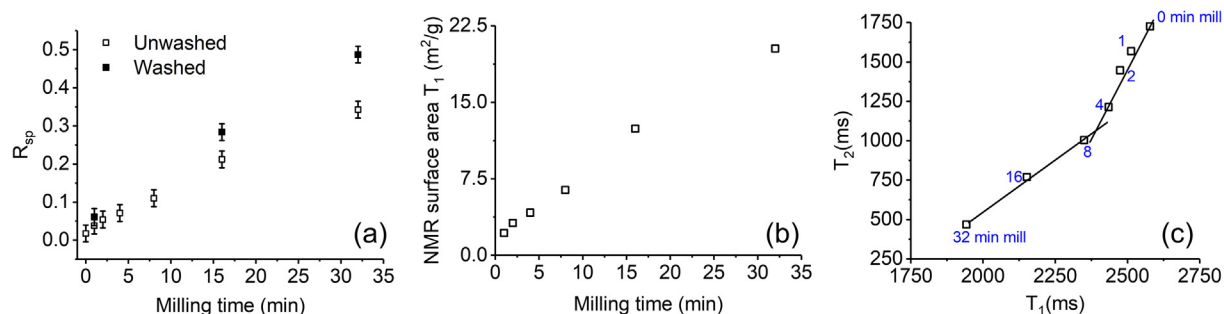
Fig. 10. (a) T_1 relaxation rate enhancement (R_{sp}) for unmilled and milled TiO_2 particles compared to bulk water ($T_{1, \, water} \sim 2600$ ms), with error bars representing the maximum standard deviation for washed and unwashed samples. (b) NMR surface area of unwashed samples calculated from T_1 and using the surface specific relaxation constants K_a (g/m^2/ms) derived from the 8-min milled BET surface area. (c) NMR relaxation time measurements T_1 and T_2 for unwashed TiO_2 particles, with lines drawn across two regions to guide the eye.

specific relaxation constant) allowing R_{sp} to be converted to particle surface area for the other milling times [58]. The 8 min milled sample was used as the reference system as it corresponds to the onset of the plateau observed in the zeta potential with increased milling time (Fig. 5 b), consistent with an increase in concentration of SHMP at the particle surface. Therefore, it was thought that after 8 min of milling, the R_{sp} would be most significantly enhanced due to the contribution of SHMP at the particle surface rather than the increased surface area available from aggregate breakage. Thus, the K_a for milled TiO_2 was calculated and correlated to the surface area obtained from the BET measurement for the 8 min milled sample, giving a K_a of 3.93×10^{-4} g/m^2/ms.

Fig. 10(b) shows the calculated surface area as a function of milling time, which compares relatively well with the BET results (Fig. 9) obtained at low milling times. However, at long milling times (16 and 32 min milling) the calculated surface areas continue increasing significantly, rather than beginning to plateau (as observed with the BET data). The deviation observed in the NMR could be due to a number of factors. Importantly, BET measures the particle surface area as a dried powder, compared to NMR where surface area measurements are performed on the dispersed suspension. Therefore, it is likely that the surface area is smaller by BET due to the presence of agglomerates compared to NMR where these are broken during sonication (see Fig. S4). However, it should be noted that the increase in surface area from agglomerate breakage is likely to be small and therefore alone cannot account for the differences. An additional explanation is the influence of the nanoparticle fines evidenced after long milling times from TEM, which at ~20 nm may contribute to much greater dispersion surface areas. Whilst the effect of these nanoparticle fines would be masked in the dried powder BET, they would be more evident in dispersion conditions. Also, as it was evident from TEM that these fines largely adsorbed onto the primary particles, it is assumed that they would increase the surface area primarily through roughening of the primary particles surfaces. Nevertheless, given the magnitude of the changes in relaxation rate after 16 and 32 milling times, it is still difficult to attribute the differences to actual surface area increases alone.

In an attempt to better understand relaxation changes with milling time, it was decided to consider both T_1 and T_2 relaxation measurements. Although both T_1 and T_2 can be used to determine particle surface area, using one or the other has both advantages and disadvantages [39]. Whilst T_2 measurements are faster, which is advantageous if samples are not stable (for example, if sedimentation occurs) the relaxation time can become very small at high suspension concentrations, leading to potential measurement errors. Furthermore, T_2 is more sensitive to changes in available surface area, and to the presence of ferromagnetic or paramagnetic impurities. Due to the differences in sensitivity of T_1 and T_2, it can

be advantageous to measure both relaxation times, as shown in Fig. 10(c). Here, a clear inflection in the data arises between the 4 and 8 min milled samples, correlated to the change in zeta potential for pigment samples (Fig. 5(b)), which plateaus after 8 min of milling, as previously conversed this is suggestive of monolayer SHMP coverage.

While it is evident that longer milling times lead to an increase in adsorption density of the SHMP, it was assumed that the adsorption plateaus post 8 min, limiting further surface chemistry contributions (as discussed). However, given the potential for extended milling times to lead to hydrolysis or other structural changes of the dispersant because of the high energy milling conditions, we may have to consider the influence of the dispersant structure in addition to the influence of its density on NMR relaxation. It may be that hydrolysed SHMP has a greater influence on NMR surface relaxation than un-modified SHMP, although, due to the convoluted nature of the overall response, it is very difficult to further define the interactions between SHMP and the bound water.

After centrifugal washing, an increase in R_{sp} was observed, as shown in Fig. 10(a), where the increase is minimal and within the measurement error for the 1 min milled sample, but this increase becomes significant with increased milling time. The first explanation is that the removed or hydrolysed polyphosphate (observed from the changes in zeta potential and phosphorus content determined using XRF; see Section 3.2) which occurs for samples milled for longer periods of time, leads to an increase in exposed alumina surface sites. Aluminium (^{27}Al) is a quadrupolar nucleus and can cause enhancements in relaxation rates of bound solvent molecules at the colloid surface [50]. However, if this was simply the case, one would expect the relaxation rate of the 1 min milled sample (unwashed or washed) to show the largest enhancements, as these samples have the lowest phosphorus content according to XRF, and should therefore have more exposed Al surface sites. For both the unwashed and washed samples milled for 16 and 32 min, the surface area increases, and the number of fines increases leading to a faster relaxation rate than the one of the washed or unwashed 1 min milled samples. As previously stated, the ball mill energy might be altering the surface structure of the dispersant or exposing further Al sites, whilst some dispersant can be washed off, this is most likely weakly interacting salt that might not contribute to the large relaxation enhancements. The remaining chemisorbed polyphosphate salt may have an altered surface structure, and this, coupled with the increase in exposure of Al surface sites, may be the reason for the enhanced relaxation rates upon washing. While it is difficult to state for certain what changes in the dispersant structure are occurring without additional surface analysis and this is an area of ongoing investigation, the degradation of an ammonium salt of poly(methacrylic acid) used during wet ball milling of alumina has previously been reported [81].

4. Conclusions

The effect of milling time on the interactions between aluminium doped titania pigment particles and polyphosphate (SHMP) dispersant has been studied using multiple characterisation techniques. TEM highlighted the presence of ~20 nm fractured fines in samples milled for 32 min that were found to have d-spacings correlating to a rutile crystal structure, implying that milling did not induce changes in crystal structure. Although the milling conditions that induced these breakage events are under high-shear, such large milling RPM, are required in order to scale down the milling process from production plant scale to lab scale. The appearance of fractured TiO_2 fines is even more significant, as many pigment production processes have similar unit operations and thus it could be assumed that many TiO_2 pigment samples may contain these fractured fines if the TiO_2 reactor discharge is milled for long times.

The TiO_2 samples were found to have an isoelectric point (iep) in the range of pH 3–4.5, with an increase in milling time leading to a lower pH_{iep}. It was proposed that increasing the milling time leads to the presence of more SHMP on the alumina-doped pigment surface, due to the breakage of agglomerates/aggregates. DLS measurements probed two relaxation modes: (i) a mode characterised by a fast relaxation time, assigned to primary TiO_2 particles, and (ii) a mode characterised by longer relaxation times, subject to inter-measurement variability, and assigned to the aggregates present in the suspensions. The hydrodynamic diameter associated with the primary TiO_2 particles did not change upon milling time, while the DLS data suggested that the proportion of aggregates in the suspensions decreased upon milling time. Interestingly also, phosphorus content and zeta potential analysis after centrifugal washing showed that SHMP was partially removed for the longer milled pigment samples, whereas no change was observed for the shorter milled samples. It was assumed that either additional SHMP adsorption or structural changes promoted with milling, resulted in a more weakly bound surface adsorbed layer that could be removed, whereas chemisorbed dispersant was stable to repeated wash cycles.

Relaxation NMR data was also used to estimate surface area changes as a function of milling time. It showed a close to linear increase in surface area, and no plateau was detected, due to either the increase in surface area from fractured fines in the samples milled for longer times, or due to the increase in SHMP concentration and/or dispersant restructuring at the surface of the titana particles. It was hypothesised that hydrolysed SHMP has a greater influence on the NMR relaxation rate of bound water molecules leading to an enhancement in $\boldsymbol{R_{sp}}$, although it is difficult to state for certain without further surface analysis of the SHMP with milling. Additionally, washed samples also resulted in larger NMR $\boldsymbol{R_{sp}}$ values for longer milling times, in comparison to the unwashed samples. Such changes were explained from either the exposure of surface alumina sites or hydrolysed SHMP after wash cycles having a greater relaxation rate than non-hydrolysed SHMP, however future work is suggested to further investigate this area. Importantly, this paper demonstrates the difficulties of characterising shear-dependent milled aggregates and the need for multiple characterisation techniques, alongside the potential of NMR relaxometry as an online-process control tool for not only detecting changes in surface area but also surface chemistry.

Data statement

The article metadata is available in the University of Leeds repository. Laura Elliott (2019): Characterisation of polyphosphate dispersant interactions with aluminium-doped titania nanoparticles during milling data set. University of Leeds. [Dataset]. https://doi.org/10.5518/576. Article metadata is available under a Creative Commons Attribution licence (CC-BY).

Appendix A. Supplementary material

Supplementary data to this article can be found online at https://doi.org/10.1016/j.jcis.2019.04.009.

References

[1] M. Gardon, J.M. Guilemany, Milestones in functional titanium dioxide thermal spray coatings: a review, J. Therm. Spray Technol. 23 (2014) 577–595.
[2] T.-H. Wang, A.M. Navarrete-Lopez, S. Li, D.A. Dixon, Hydrolysis of TiCl4, initial steps in the production of TiO2, J. Phys. Chem. A 114 (2010) 7561–7570.
[3] L. Zhao, Y. Liu, L. Wang, H. Zhao, D. Chen, B. Zhong, J. Wang, T. Qi, Production of rutile TiO2 pigment from titanium slag obtained by hydrochloric acid leaching of vanadium-bearing titanomagnetite, Ind. Eng. Chem. Res. 53 (2014) 70–77.
[4] X. Xiong, Z. Wang, F. Wu, X. Li, H. Guo, Preparation of TiO2 from ilmenite using sulfuric acid decomposition of the titania residue combined with separation of Fe3+ with EDTA during hydrolysis, Adv. Powder Technol. 24 (2013) 60–67.
[5] W. Zhang, Z. Zhu, C.Y. Cheng, A literature review of titanium metallurgical processes, Hydrometallurgy 108 (2011) 177–188.
[6] G.S. McNulty, Production of Titanium Dioxide, IAEA, International Atomic Energy Agency (IAEA), 2008.
[7] Zion, Titanium Dioxide Market for Paints & Coatings, Plastic, Paper and Other Applications: Global Industry Perspective, Comprehensive Analysis, Size, Share, Growth, Segment, Trends and Forecast, 2014–2020, 2016, pp. 110.
[8] J.H. Braun, A. Baidins, R.E. Marganski, TiO2 pigment technology: a review, Prog. Org. Coat. 20 (1992) 105–138.
[9] A. Hartmann, Process for the use of rutile promoter and control additives in the manufacture of titanium dioxide by the chloride process, Google Patents (1996).
[10] M.K. Akhtar, Y. Xiong, S.E. Pratsinis, Vapor synthesis of titania powder by titanium tetrachloride oxidation, AlChE J. 37 (1991) 1561–1570.
[11] K. Akhtar, S. Pratsinis, S. Mastrangelo, Vapor phase synthesis of Al-doped titania powders, J. Mater. Res. 5 (1994) 1241–1249.
[12] J.P.B. Manuel, Jesús Gázquez, Rafael Garcia-Tenorio, Federico Vaca, A review of the production cycle of titanium dioxide pigment, Mater. Sci. Appl. 5 (2014) 441–458.
[13] E. Castellini, C. Berthold, D. Malferrari, F. Bernini, Sodium hexametaphosphate interaction with 2:1 clay minerals illite and montmorillonite, Appl. Clay Sci. 83–84 (2013) 162–170.
[14] E. Castellini, G. Lusvardi, G. Malavasi, L. Menabue, Thermodynamic aspects of the adsorption of hexametaphosphate on kaolinite, J. Colloid Interface Sci. 292 (2005) 322–329.
[15] Y. Han, W. Liu, J. Zhou, J. Chen, Interactions between kaolinite AlOH surface and sodium hexametaphosphate, Appl. Surf. Sci. 387 (2016) 759–765.
[16] Y. Wang, E. Forssberg, Dispersants in stirred ball mill grinding, Kona Powder Part. J. 13 (1995) 67–77.
[17] M.L. Taylor, G.E. Morris, R.S.C. Smart, Polyphosphate interaction with aluminium-doped titania pigment particles, Colloids Surf., A 190 (2001) 285–294.
[18] A. Feiler, P. Jenkins, J. Ralston, Metal oxide surfaces separated by aqueous solutions of linear polyphosphates: DLVO and non-DLVO interaction forces, PCCP 2 (2000) 5678–5683.
[19] A. Michelmore, W. Gong, P. Jenkins, J. Ralston, The interaction of linear polyphosphates with titanium dioxide surfaces, PCCP 2 (2000) 2985–2992.
[20] P.A. Connor, A.J. McQuillan, Phosphate adsorption onto TiO2 from aqueous solutions: an in situ internal reflection infrared spectroscopic study, Langmuir 15 (1999) 2916–2921.
[21] C. Rulliere, L. Perenes, D. Senocq, A. Dodi, S. Marchesseau, Heat treatment effect on polyphosphate chain length in aqueous and calcium solutions, Food Chem. 134 (2012) 712–716.

[22] N. Cini, V. Ball, Polyphosphates as inorganic polyelectrolytes interacting with oppositely charged ions, polymers and deposited on surfaces: fundamentals and applications, Adv. Colloid Interface Sci. 209 (2014) 84–97.

[23] F. Rashchi, J.A. Finch, Polyphosphates: a review their chemistry and application with particular reference to mineral processing, Miner. Eng. 13 (2000) 1019–1035.

[24] S. Farrokhpay, G.E. Morris, D. Fornasiero, P. Self, Influence of polymer functional group architecture on titania pigment dispersion, Colloids Surf., A 253 (2005) 183–191.

[25] S. Farrokhpay, G.E. Morris, D. Fornasiero, P. Self, Stabilisation of titania pigment particles with anionic polymeric dispersants, Powder Technol. 202 (2010) 143–150.

[26] S. Farrokhpay, G.E. Morris, L.G. Britcher, Stability of sodium polyphosphate dispersants in mineral processing applications, Miner. Eng. 39 (2012) 39–44.

[27] M. He, Y. Wang, E. Forssberg, Slurry rheology in wet ultrafine grinding of industrial minerals: a review, Powder Technol. 147 (2004) 94–112.

[28] C. Lindberg, J. Akroyd, M. Kraft, Developing breakage models relating morphological data to the milling behaviour of flame synthesised titania particles, Chem. Eng. Sci. 166 (2017) 53–65.

[29] K. Ohenoja, M. Illikainen, J. Niinimäki, Effect of operational parameters and stress energies on the particle size distribution of TiO2 pigment in stirred media milling, Powder Technol. 234 (2013) 91–96.

[30] H. Bel Fadhel, C. Frances, A. Mamourian, Investigations on ultra-fine grinding of titanium dioxide in a stirred media mill, Powder Technol. 105 (1999) 362–373.

[31] M. Inkyo, T. Tahara, T. Iwaki, F. Iskandar, C.J. Hogan, K. Okuyama, Experimental investigation of nanoparticle dispersion by beads milling with centrifugal bead separation, J. Colloid Interface Sci. 304 (2006) 535–540.

[32] S. Jeon, T. Thajudeen, C.J. Hogan, Evaluation of nanoparticle aggregate morphology during wet milling, Powder Technol. 272 (2015) 75–84.

[33] S. Bégin-Colin, T. Girot, G. Le Caër, A. Mocellin, Kinetics and mechanisms of phase transformations induced by ball-milling in anatase TiO2, J. Solid State Chem. 149 (2000) 41–48.

[34] A. Gajović, M. Stubičar, M. Ivanda, K. Furić, Raman spectroscopy of ball-milled TiO2, J. Mol. Struct. 563 (2001) 315–320.

[35] S. Sen, M.L. Ram, S. Roy, B.K. Sarkar, The structural transformation of anatase TiO2 by high-energy vibrational ball milling, J. Mater. Res. 14 (2011) 841–848.

[36] V. Sepelak, S. Begin-Colin, G. Le Caer, Transformations in oxides induced by high-energy ball-milling, Dalton Trans. 41 (2012) 11927–11948.

[37] W. Schärtl, Light Scattering from Polymer Solutions and Nanoparticle Dispersions, Springer, Berlin Heidelberg, 2007.

[38] Z.E. Allouni, M.R. Cimpan, P.J. Høl, T. Skodvin, N.R. Gjerdet, Agglomeration and sedimentation of TiO2 nanoparticles in cell culture medium, Colloids Surf. B: Biointerfaces 68 (2009) 83–87.

[39] D. Fairhurst, T. Cosgrove, S.W. Prescott, Relaxation NMR as a tool to study the dispersion and formulation behavior of nanostructured carbon materials, Magn. Reson. Chem. 54 (2016) 521–526.

[40] T.C. Catherine, L. Cooper, Jeroen S. van Duijneveldt, Martin Murray, Stuart W. Prescott, The use of solvent relaxation NMR to study colloidal suspensions, Soft Matter 9 (2013) 7211.

[41] C.L. Cooper, T. Cosgrove, J.S. van Duijneveldt, M. Murray, S.W. Prescott, Colloidal particles in competition for stabilizer: a solvent relaxation NMR study of polymer adsorption and desorption, Langmuir 28 (2012) 16588–16595.

[42] C.L. Cooper, T. Cosgrove, J.S. van Duijneveldt, M. Murray, S.W. Prescott, Competition between polymers for adsorption on silica: a solvent relaxation NMR and small-angle neutron scattering study, Langmuir 29 (2013) 12670–12678.

[43] C. Flood, T. Cosgrove, I. Howell, P. Revell, Effects of electrolytes on adsorbed polymer layers: poly(ethylene oxide)–silica system, Langmuir 22 (2006) 6923–6930.

[44] C. Flood, T. Cosgrove, Y. Espidel, I. Howell, P. Revell, Effects of surfactants and electrolytes on adsorbed layers and particle stability, Langmuir 24 (2008) 7323–7328.

[45] C. Flood, T. Cosgrove, D. Qiu, Y. Espidel, I. Howell, P. Revell, Influence of a surfactant and electrolytes on adsorbed polymer layers, Langmuir 23 (2007) 2408–2413.

[46] A. Nelson, K.S. Jack, T. Cosgrove, D. Kozak, NMR solvent relaxation in studies of multicomponent polymer adsorption, Langmuir 18 (2002) 2750–2755.

[47] G.P. Van der Beek, M.A.C. Stuart, T. Cosgrove, Polymer adsorption and desorption studies via proton NMR relaxation of the solvent, Langmuir 7 (1991) 327–334.

[48] C. Flood, T. Cosgrove, Y. Espidel, I. Howell, P. Revell, Sodium polyacrylate adsorption onto anionic and cationic silica in the presence of salts, Langmuir 23 (2007) 6191–6197.

[49] T. Cosgrove, T.M. Obey, M. Taylor, Solvent relaxation NMR: bound fraction determination for sodium poly(styrene sulphonate) at the solid/solution interface, Colloids Surf. 64 (1992) 311–316.

[50] C.L. Cooper, T. Cosgrove, J.S. van Duijneveldt, M. Murray, S.W. Prescott, The use of solvent relaxation NMR to study colloidal suspensions, Soft Matter 9 (2013) 7211–7228.

[51] C. Terenzi, C. Casieri, F. De Luca, R. Quaresima, G. Quarta, V. Tudisca, Firing-induced microstructural properties of quasi-diamagnetic carbonate-based porous ceramics: a 1H NMR relaxation correlation study, Appl. Magn. Reson. 46 (2015) 1159–1178.

[52] X. Li, Y. Li, C. Chen, D. Zhao, X. Wang, L. Zhao, H. Shi, G. Ma, Z. Su, Pore size analysis from low field NMR spin–spin relaxation measurements of porous microspheres, J. Porous Mater. 22 (2015) 11–20.

[53] D.P. Gallegos, D.M. Smith, C.J. Brinker, An NMR technique for the analysis of pore structure: application to mesopores and micropores, J. Colloid Interface Sci. 124 (1988) 186–198.

[54] D.P. Gallegos, K. Munn, D.M. Smith, D.L. Stermer, A NMR technique for the analysis of pore structure: application to materials with well-defined pore structure, J. Colloid Interface Sci. 119 (1987) 127–140.

[55] S.B. Thoma, D.M. Smith, J. Boughton, R. Davies, On-line surface area measurement of concentrated slurries using low field spin-lattice relaxation NMR, Part. Part. Syst. Char. 10 (1993) 246–251.

[56] P.J. Davis, D.P. Gallegos, D.M. Smith, Rapid surface area determination via NMR spin-lattice relaxation measurements, Powder Technol. 53 (1987) 39–47.

[57] C.L. Glaves, P.J. Davis, D.M. Smith, Surface area determination via NMR: fluid and frequency effects, Powder Technol. 54 (1988) 261–269.

[58] L.N. Elliott, R.A. Bourne, A. Hassanpour, J.L. Edwards, S. Sutcliffe, T.N. Hunter, Salt enhanced solvent relaxation and particle surface area determination via rapid spin-lattice NMR, Powder Technol. 333 (2018) 458–467.

[59] C.A. Schneider, W.S. Rasband, K.W. Eliceiri, NIH Image to ImageJ: 25 years of image analysis, Nat. Meth. 9 (2012) 671–675.

[60] N. Hondow, R. Brydson, P. Wang, M.D. Holton, M.R. Brown, P. Rees, H.D. Summers, A. Brown, Quantitative characterization of nanoparticle agglomeration within biological media, J. Nanopart. Res. 14 (2012) 977.

[61] M. Horn, C.F. Schwerdtfeger, E.P. Meagher, Refinement of the structure of anatase at several temperatures, Zeitschrift fur Kristallographie (1972) 273–281.

[62] M.S.U. Okrusch, R. Hock, A. Brummer, H. Theisinger, M. Baier, Intergrown niobian rutile phases with Sc- and W-rich ferrocolumbite: an electron-microprobe and Rietveld study, Am. Mineral. (2003) 986–995.

[63] A.L. Patterson, The Scherrer formula for X-ray particle size determination, Phys. Rev. 56 (1939) 978–982.

[64] J.S. Behra, J. Mattsson, O.J. Cayre, E.S.J. Robles, H. Tang, T.N. Hunter, Characterization of sodium carboxymethyl cellulose aqueous solutions to support product formulation: a rheology and light scattering study, ACS Appl. Polym. Mater. 1 (2019) 344–358.

[65] V. Jordan, U. Javornik, J. Plavec, A. Podgornik, A. Rečnik, Self-assembly of multilevel branched rutile-type TiO(2) structures via oriented lateral and twin attachment, Sci. Rep. 6 (2016) 24216.

[66] S.M. Klein, J.H. Choi, D.J. Pine, F.F. Lange, Synthesis of rutile titania powders: agglomeration, dissolution, and reprecipitation phenomena, J. Mater. Res. 18 (2011) 1457–1464.

[67] N. Mandzy, E. Grulke, T. Druffel, Breakage of TiO2 agglomerates in electrostatically stabilized aqueous dispersions, Powder Technol. 160 (2005) 121–126.

[68] A. Gajovic, K. Furic, S. Music, Ball-Milling of TiO2 and ZrO2, Rudjer Boskovic Institute, Bijenicka, 54 10000.

[69] J.D. Dana, Manual of Mineralogy, Durrie & Peck, 1855.

[70] T.A. Egerton, I.R. Tooley, Physical characterization of titanium dioxide nanoparticles, Int. J. Cosmet. Sci. 36 (2014) 195–206.

[71] M.L. Taylor, G.E. Morris, R.S.C. Smart, Influence of aluminum doping on titania pigment structural and dispersion properties, J. Colloid Interface Sci. 262 (2003) 81–88.

[72] P. McFadyen, D. Fairhurst, High-resolution particle size analysis from nanometres to microns, Clay Miner. 28 (1993) 531–537.

[73] J. Shiels, D. Harbottle, T.N. Hunter, Synthesis and physical property characterisation of spheroidal and cuboidal nuclear waste simulant dispersions, Materials 11 (2018) 1235.

[74] N. Paul, S. Biggs, J. Shiels, R. Hammond, M. Edmondson, L. Maxwell, D. Harbottle, T. Hunter, Influence of shape and surface charge on the sedimentation of spheroidal, cubic and rectangular cuboid particles, Powder Technology (2017).

[75] M. Johnson, J. Peakall, M. Fairweather, S. Biggs, D. Harbottle, T.N. Hunter, Characterization of multiple hindered settling regimes in aggregated mineral suspensions, Ind. Eng. Chem. Res. 55 (2016) 9983–9993.

[76] U. Gesenhues, Substructure of titanium dioxide agglomerates from dry ball-milling experiments, J. Nanopart. Res. 1 (1999) 223–234.

[77] F. Karakaş, M.S. Çelik, Mechanism of TiO2 stabilization by low molecular weight NaPAA in reference to water-borne paint suspensions, Colloids Surf., A 434 (2013) 185–193.

[78] N.S. Allen, M. Edge, A. Ortega, G. Sandoval, C.M. Liauw, J. Verran, J. Stratton, R.B. McIntyre, Degradation and stabilisation of polymers and coatings: nano versus pigmentary titania particles, Polym. Degrad. Stab. 85 (2004) 927–946.

[79] S. Fazio, J. Guzmán, M.T. Colomer, A. Salomoni, R. Moreno, Colloidal stability of nanosized titania aqueous suspensions, J. Eur. Ceram. Soc. 28 (2008) 2171–2176.

[80] G. Mestl, B. Herzog, R. Schloegl, H. Knoezinger, Mechanically activated MoO3. 1. Particle size, crystallinity, and morphology, Langmuir 11 (1995) 3027–3034.

[81] T. Chartier, S. Souchard, J.F. Baumard, H. Vesteghem, Degradation of dispersant during milling, J. Eur. Ceram. Soc. 16 (1996) 1283–1291.